DOI: 10.1002/((please add manuscript number))
Article type: Full Paper

Sulphur-Deficient Bismuth Sulfide/Nitrogen-Doped Carbon Nanofibers as Advanced Free-Standing Electrode for Asymmetric Supercapacitors

Wei Zong, Feili Lai, Guanjie He, Jianrui Feng, Wei Wang, Ruqian Lian, Yue-E Miao, Gui-Chang Wang, Ivan P. Parkin, and Tianxi Liu**

W. Zong, F. L. Lai, Y. E. Miao, T. X. Liu
State Key Laboratory for Modification of Chemical Fibers and Polymer Materials, College of Materials Science and Engineering, Innovation Center for Textile Science and Technology,
Donghua University
Shanghai 201620, P. R. China
Email: txliu@dhu.edu.cn or fllai14@fudan.edu.cn

G. J. He, I. P. Parkin
Christopher Ingold Laboratory, Department of Chemistry
University College London
20 Gordon Street, London WC1H 0AJ, U.K.

J. R. Feng, G. C. Wang
College of Chemistry, Key Laboratory of Advanced Energy Materials Chemistry (Ministry of Education)
Nankai University
Tianjin 300071, P. R. China

W. Wang
Department of Materials Science and Engineering, College of Engineering
Peking University
Beijing 100871, P. R. China

R. Q. Lian
College of Physics
Jilin University
Changchun 130012, P. R. China

Keywords: sulphur deficiency, bismuth sulfides, nitrogen-doped carbon nanofibers, free-standing, asymmetric supercapacitor

The use of free-standing carbon-based hybrids plays a crucial role to help fulfil

ever-increasing energy storage demands, but is greatly hindered by the limited number of active sites for fast charge adsorption/desorption processes. Herein, an efficient strategy is demonstrated for making defect-rich bismuth sulfides in combination with surface nitrogen-doped carbon nanofibers (dr-Bi_2S_3/S-NCNF) as flexible free-standing electrodes for asymmetric supercapacitors. The dr-Bi_2S_3/S-NCNF composite exhibits superior electrochemical performances with an enhanced specific capacitance of 466 F g^{-1} at a discharge current density of 1 A g^{-1}. The high performance of dr-Bi_2S_3/S-NCNF electrodes originates from its hierarchical structure of nitrogen-doped carbon nanofibers with well anchored defect-rich bismuth sulfides nanostructures. As modelled by density functional theory calculation, the dr-Bi_2S_3/S-NCNF electrodes exhibit reduced OH^- adsorption energy of -3.15 eV, compared with that (-3.06 eV) of defect-free bismuth sulfides/surface nitrogen-doped carbon nanofiber (df-Bi_2S_3/S-NCNF). An asymmetric supercapacitor was successfully assembled by using dr-Bi_2S_3/S-NCNF composite as the negative electrode and S-NCNF as the positive electrode materials. This composite exhibits a high energy density of 22.2 Wh kg^{-1} at a power density of 677.3 W kg^{-1}. This work demonstrates a feasible strategy to construct advanced metal sulfide-based free-standing electrodes by incorporating defect-rich structures using surface engineering principles.

1. Introduction

Nowadays, ever-increasing environmental pollution and energy shortage requirement have triggered tremendous concerns and global explorations to develop efficient energy conversion and storage systems, such as electrochemical water splitting,

electroreduction of CO_2, innovative batteries and supercapacitors.[1-5] Among them, supercapacitors, especially pseudocapacitors, have attracted wide attention and been regarded as one of the most perspective energy storage systems due to their high power/energy density and fast charge/discharge processes. Bismuth chalcogenides (Bi_2X_3, where X = O, S, Se) are a species of electrode materials employed in pseudocapacitors as they have multiply intrinsic characteristics of environmental friendliness, low cost and natural abundance. Bismuth sulfide (Bi_2S_3), for example, has a narrow bandgap of 1.3 eV and high dielectric permittivity, making it potential candidate for supercapacitor electrodes. However, the electrochemical energy storage performance of bismuth sulfides is confined by their low electrical conductivity and limited number of active sites, which stems from their poor electron transfer ability and severe self-aggregation or even complete crystal/atomic structure.[6-8]

Recent studies illustrate that vacancy/defect engineering on the surface of metal sulfide/oxide is a potentially effective approach to achieve more active sites for surface redox reaction and faster charge transfer ability in electrodes.[9-11] For instance, Liu *et al.*[12] prepared a flexible electrode of oxygen-defect bismuth oxide/graphene supported on bacterial cellulose by combined solvothermal and reduction processes to deliver an improved capacitance of 1137 F g^{-1} (based on oxygen-defect Bi_2O_3 active material). Zhai *et al.*[13] demonstrated that oxygen-deficient MnO_2 nanorods show a superior areal capacitance of 449 F g^{-1} with excellent rate capability and cycling stability, which is much more outstanding than that (96.2 F g^{-1}) of pure MnO_2 nanorods. To reveal the function of sulphur deficiency in Bi_2S_3, density functional

theory (DFT) calculations are applied as a guide before the experiments. As shown in Figure 1a, the sulphur-deficient Bi_2S_3 exhibits obviously enhanced density of states (DOS) at the conduction band edge as compared to its pristine counterpart, which is beneficial to achieve promoted electrical conductivity. Meanwhile, the charge distribution in sulphur-deficient Bi_2S_3 is significantly disturbed after incorporation of sulphur-deficiency in Bi_2S_3 crystal. As shown in Figure 1b, the charge densities around sulphur deficiency and neighboring bismuth atoms are weakened and enhanced, respectively, and this differential charge distribution can provide more active sites for electrochemical reactions.

Except for sulphur deficiency engineering in Bi_2S_3, constructing novel nanostructures can increase its specific surface area to provide more active sites. Our previous works have reported an effective strategy to fabricate advanced supercapacitor electrodes by constructing three-dimensional (3D) networks between pseudo-capacitive compound and porous conductive carbon nanofiber substrate.[14-16] Here, electrospinning is a mature and low-cost technique to fabricate 3D networks by stacking thousands of one-dimensional randomly oriented nanofibers, which can be controlled and easily tailored (such as nanofiber diameter and surface tomography). By using an easily-controlled carbonization process, well maintained 3D carbon nanofiber networks can be obtained as templates for uniform dispersion of Bi_2S_3 nanostructures. This strategy can endow Bi_2S_3 nanostructures with remarkable electrical inter-connection and mechanical integrity, leading to enhanced electrical conductivity and increased active sites for high-performance free-standing electrodes

in supercapacitors. Furthermore, the tactic of doping, such as nitrogen, sulfide, phosphorus, and oxygen atoms, can regulate the atomic-scale defects of sp^3 carbons to obtain better interfacial connections between carbon nanofibers and Bi_2S_3 nanoparticles for a higher interfacial charge transfer rate. In particular, the nitrogen heteroatom has been demonstrated as a popular platform to tune the valence orbital energy levels between neighboring carbons, resulting in enhanced storage capability.[17-22]

In this work, we report a facile way to prepare defect-rich bismuth sulfides/surface nitrogen-doped carbon nanofibers (dr-Bi_2S_3/S-NCNF) as a flexible free-standing electrode for asymmetric supercapacitors. The dr-Bi_2S_3/S-NCNF composite exhibits a superior electrochemical performance owing to its unique structures, consisting of surface nitrogen-doped carbon nanofiber support that is uniformly covered by defect-rich bismuth sulfides nanoparticles. As the adsorption of electrolyte ions mainly happens on the outer surface of the materials, the S-NCNF electrode with more N-doped active sites on the surface of the carbon nanofibers exhibits an enhanced specific capacitance (280.1 F g^{-1} at 1 A g^{-1}), by approximately 3 times compared with a pure carbon nanofiber electrode (about 82 F g^{-1} at 1 A g^{-1}). In addition, the dr-Bi_2S_3/S-NCNF composite displays enhanced specific capacitance of 466 F g^{-1} at a discharge current density of 1 A g^{-1}, high capacitance retention of 64.1% even at a high discharge current density of 8 A g^{-1}, and excellent cycling stability of 81.5% after 1000 cycles. This high performance of dr-Bi_2S_3/S-NCNF electrode is due to the successful introduction of abundant defects into the surface of bismuth sulfides,

which facilitates absorption of electrolyte ions with a reduced OH^- adsorption energy of -3.15 eV than that (-3.06 eV) of defect-free bismuth sulfides/surface nitrogen-doped carbon nanofiber (df-Bi_2S_3/S-NCNF). As a result, the asymmetric supercapacitor, by using dr-Bi_2S_3/S-NCNF composite as a negative electrode and S-NCNF carbon nanofibers as a positive electrode, shows a wider potential window of 0 ~ 1.35 V and a high energy density of 22.2 W h kg^{-1} at a power density of 677.3 W kg^{-1}, demonstrating its potential for application in high-performance energy storage devices.

2. Results and discussion

The synthesis process to make defect-rich bismuth sulfides/surface nitrogen-doped carbon nanofibers (dr-Bi_2S_3/S-NCNF) is illustrated in Figure 2a. The electrospun urea-containing polyacrylonitrile (u-PAN) nanofibers were firstly pre-oxidized, and further carbonized with additional urea under a N_2 flow, to obtain surface nitrogen-doped carbon nanofibers (S-NCNF). Due to the nitrogen-rich structure of S-NCNF, the Bi_2S_3 precursor can be easily adsorbed on their surfaces. The defect-free bismuth sulfides/surface nitrogen-doped carbon nanofibers (df-Bi_2S_3/S-NCNF) were synthesized via a simple solvothermal method, while the dr-Bi_2S_3/S-NCNF composite was achieved after high-temperature annealing treatment to boost the sulphur substoichiometric. Field-emission scanning electron microscopy (FESEM) was employed to study the morphologies of dr-Bi_2S_3/S-NCNF composite, as well as the S-NCNF and df-Bi_2S_3/S-NCNF composite. As shown in Figure 2b, the electrospun

u-PAN nanofibers have an average diameter of about 800-900 nm. After successive pre-oxidation and carbonization, the average diameter of the electrospun u-PAN nanofibers is reduced to 400-500 nm, thus forming S-NCNF (Figure 2c, 2d). More importantly, thousands of surface nitrogen-doped carbon nanofibers are netted with each other to form a well-connected three-dimensional (3D) network. This porous 3D network with abundant nitrogen-doping on the carbon nanofiber surfaces not only enhances the ion diffusion ability in the inner space but also provides more electrochemically active sites for electrolyte adsorption. This implies that it has potential for outstanding energy storage performance when being incorporated into a supercapacitor. Moreover, the interconnected 3D architecture acts as a mechanically robust substrate for uniform growth of bismuth sulfide. In order to modify the electrochemical performance of hydrothermally synthesized df-Bi_2S_3/S-NCNF composite, a further annealing process was applied under a nitrogen atmosphere to introduce abundant sulphur defects on the surface of the dr-Bi_2S_3/S-NCNF composite. As shown in the SEM images in Figure 2e and 2f, the dr-Bi_2S_3 nanoparticles are still uniformly coated on the surface of S-NCNF, similar to df-Bi_2S_3/S-NCNF composite (inset in Figure 2e), revealing the success of annealing treatment without obvious distortion of the morphology. Further, the energy-dispersive X-ray spectroscopy (EDS) mapping images (Figure S2) demonstrate the homogeneous spatial distribution of N, Bi, and S in the basal carbon nanofibers. More importantly, the as-treated dr-Bi_2S_3/S-NCNF composite membrane exhibits extraordinary flexibility (inset in Figure 2f) and can be used directly as an electrode in a supercapacitor. To further

investigate the crystal structure of the as-prepared dr-Bi_2S_3/S-NCNF, high-resolution transmission electron microscopy (HR-TEM) analysis was performed. The clear lattice fringes shown in Figure 2g have an interplanar spacing of 0.36 nm, which is attributed to the (130) plane of Bi_2S_3 nanoparticles.

To confirm the phase structure of the different materials, the X-ray diffraction (XRD) patterns are shown in Figure 3a. The dr-Bi_2S_3/S-NCNF, df-Bi_2S_3/S-NCNF composites, and pure Bi_2S_3 aggregates display four distinct characteristic peaks at 2θ = 13.2°, 31.9°, 38.1°, and 46.2°, corresponding to the (130), (211), (221), and (431) crystal planes of Bi_2S_3 (JCPDS Card no. 00-017-0320), respectively.[23] Furthermore, a broad peak ranging from 2θ = 20° to 30° was observed in the XRD pattern of Bi_2S_3/S-NCNF composite, which is attributed to the amorphous carbon nanofibers (JCPDS Card no. 01-0646). The surface compositions of the different samples are also reflected in their Raman spectra as shown in Figure S3. The I_D/I_G ratios show the degrees of defects in carbonaceous materials for S-NCNF, NCNF and pure CNF are 2.05, 1.79 and 1.49, respectively (Figure S3). The computational results indicate that the S-NCNF possesses more disorders or defects than those of the NCNF and pure CNF, resulting from the incorporation of more N-doped active sites on the surface of the carbon nanofibers.[24] X-ray photoelectron spectroscopy (XPS) was utilized to investigate the surface chemical compositions and valence states of the dr-Bi_2S_3/NCNF composite, as well as the S-NCNF. The full-survey-scan spectrum (Figure 3b) exhibits the characteristic peaks for C, N, O, S, and Bi as the principal elemental components. According to the XPS, the N 1s spectrum (Figure 3c) shows

that the nitrogen atom has been incorporated into the surface of carbon nanofibers and is mainly present in three forms centered at 398.4 eV, 399.8 eV and 401.1 eV, corresponding to the pyridine-like (N-6), pyrrolic-like (N-5), and graphitic-like (N-Q) nitrogens, respectively.[25] The nitrogen atom % contents in pure CNF, NCNF and S-NCNF were calculated to be 2.27%, 4.08% and 6.99%, respectively (Figure S4c). Meanwhile, the portions of each N-configuration within pure CNF, NCNF and S-NCNF are shown graphically in Figure S4d. The results demonstrate that S-NCNF has achieved an inhomogenous nitrogen-doped carbon nanofiber structure with relatively poor nitrogen-doping and rich nitrogen-doping inside the carbon nanofibers and on the surface of carbon nanofibers, respectively. This unique nitrogen-doped carbon nanofibers are totally different from the nitrogen-doped carbon materials reported previously,[26,27] proving the superiority of the two-step nitrogen-doping processes, which is beneficial to enhance its energy storage performance due to the extra active sites on the surface of the carbon nanofibers. Apart from the S 2p peak (Figure 3d), both dr-Bi_2S_3/S-NCNF and df-Bi_2S_3/S-NCNF composites also show several peaks belonging to Bi 4f (Bi $4f_{5/2}$: 159.3 and 164.6 eV; Bi $4f_{7/2}$: 163.6 and 158.3 eV).[28] This provides direct evidence of the successful formation of Bi_2S_3. It should be noted that both S $2p_{3/2}$ and S $2p_{1/2}$ peaks of the dr-Bi_2S_3/S-NCNF composite (Figure 3d) move to relatively lower binding energies with an energy shift of 0.1 eV, indicating the successful incorporation of sulphur deficiencies in the dr-Bi_2S_3/S-NCNF composite.[29-31] In comparison, there are no discernible variations in the Bi 4f peak, indicating no deficiency of Bi atoms in the dr-Bi_2S_3/S-NCNF

composite. In order to further study the quantity of sulphur deficiencies, the S/Bi atom ratios in both dr-Bi_2S_3/S-NCNF and df-Bi_2S_3/S-NCNF composites were determined from the XPS data. As shown in Figure S5, we found that the atom ratio of the S/Bi in df-Bi_2S_3/S-NCNF composite is fixed to 1.51, which matches well with defect-free Bi_2S_3 crystal. This value decreases to 1.28 for dr-Bi_2S_3/S-NCNF composite after high-temperature annealing treatment, providing convincing evidence for the presence of sulphur deficiencies in the dr-Bi_2S_3/S-NCNF composite.

The electrochemical behaviors of S-NCNF, df-Bi_2S_3/S-NCNF and dr-Bi_2S_3/S-NCNF electrodes were firstly evaluated under a three-electrode system by using 6 M KOH aqueous solution as an electrolyte. As shown in Figure 4a, cyclic voltammograms (CV) curves of various carbon nanofiber electrodes (*i.e.* pure CNF, NCNF, S-NCNF) display near-rectangular shapes at a scan rate of 20 mV s^{-1}, suggesting that the capacitance mainly arises from the ion adsorption/desorption on the surface of carbon nanofibers. In contrast with the CV curves of pure CNF and NCNF electrodes, the S-NCNF electrode shows a larger CV area, which indicates its much larger capacitance. It is because of the plentiful N-doped species on the carbon nanofibers can tune its surface valence orbital energy levels, to provide more active sites for enhanced ion adsorption/diffusion ability. Moreover, the CV curves of the S-NCNF electrode exhibits excellent shape preservation even at a high scan rate of 200 mV s^{-1} (Figure 4b), indicating its good rate stability. Linear galvanostatic charge-discharge curves of S-NCNF electrode at various current densities are shown in Figure 4c, from which the specific capacitance can be calculated to be 280.1 F g^{-1}

at 1 A g^{-1}. This high performance is superior or comparable with previously reported values of carbon-based electrodes, such as nitrogen-doped porous carbon nanofibers (245 F g^{-1} at 1 A g^{-1}),[32] metal-organic framework derived carbons (251 F g^{-1} at 5 mV s^{-1}),[33] nitrogen-doped graphene aerogels (223 F g^{-1} at 0.2 A g^{-1}) [34] and 3D porous framework-like N-doped carbon (260 F g^{-1} at 1 A g^{-1}).[35] As shown in Figure 4d, acceptable capacitance retention is observed for the S-NCNF electrode when the current density were increased to 8 A g^{-1}, which is even better than that (49.7%) for the pure CNF electrode. Further, no obvious decrease is observed after 5000 cycles at a constant scan rate of 200 mV s^{-1}, showing outstanding capacitance retention above 97% (Figure S7). These results mean that the two-step nitrogen-doping process is a novel and efficient method to boost the overall performance of carbon-based materials towards supercapacitors.

To go further, the CV curves of dr-Bi_2S_3/S-NCNF electrode at different scan rates ranged from 5 to 100 mV s^{-1} are shown in Figure 5a, from which obvious characteristic redox peaks of Bi_2S_3 are observed at a potential window of -0.95 ~ -0.4 V. In addition, the voltage plateaus at -0.8 ~ -0.7 V in the galvanostatic charge-discharge curves of dr-Bi_2S_3/S-NCNF electrode (Figure 5b) reveal its typical pseudocapacitive behaviors. The specific capacitance was calculated to be 466 F g^{-1} at a discharge current density of 1 A g^{-1}, which is considerable compared to the Bi_2S_3-based electrodes reported previously (Table S1), such as Bi_2S_3 nanorods-reduced graphene oxide nanosheet composites (396 F g^{-1} at 1 A g^{-1}),[36] Bi_2S_3/PbS solid solution in nanocomposites (402.4 F g^{-1} at 1 mA cm^{-2}),[37] and Bi_2S_3 nanorods (290 F g^{-1} at 1 A g^{-1}).[38] Furthermore, even at a high current density of 8 A g^{-1}, 64.2% (299 F g^{-1}) of the initial capacitance is still retained for dr-Bi_2S_3/S-NCNF

electrode (Figure 5c), indicating its acceptable rate capability. Nyquist plots of S-NCNF, df-Bi_2S_3/S-NCNF, and dr-Bi_2S_3/S-NCNF electrodes are shown in Figure 5d. The electrochemical impedance spectroscopy (EIS) measurements were carried out at the open-circuit potential in the frequency range from 100 kHz to 0.01 Hz. Compared to the df-Bi_2S_3/S-NCNF electrode, the dr-Bi_2S_3/S-NCNF electrode shows a reduced charge-transfer resistance in the high-frequency region, indicating their fast ion diffusion and low charge-transfer resistance. Cycling stability is another standard to evaluate the property of an electrode material. The CV curve at a current density of 200 mV s^{-1} for 1100 cycles is shown in Figure 5e. The result shows that the capacitance retention increases in the first 500 cycles owing to an activation process, and even remains at 81.5% of the initial capacitance after 1000 cycles, indicating its outstanding cycling stability for long time usage.

Compared with a df-Bi_2S_3/S-NCNF electrode, the dr-Bi_2S_3/S-NCNF electrode exhibits an enhanced electrochemical performance of higher specific capacitance, higher rate stability, and lower resistance, which can be attributed to the following reasons. Firstly, the synergistic effect of uniform dispersion of defect-rich bismuth sulfide on the surface of nitrogen-doped carbon nanofibers (Figure 5f), results into an increased specific surface area, which can maximize the contact area of the active material and electrolyte. Secondly, a slight peak shift of about 39 mV is observed for a dr-Bi_2S_3/S-NCNF electrode (Figure 5g), indicating its better reversibility in the redox processes than that of a df-Bi_2S_3/S-NCNF electrode, which is ascribed to the successful incorporation of sulphur deficiencies on its surface for faster electrolyte ion adsorption. This sulphur deficiencies derived advantage is also revealed by the density functional theory calculation. As shown in Figure 5h, the dr-Bi_2S_3/S-NCNF exhibits much lower OH^- ion adsorption energy of -3.15 eV than that (-3.06 eV) of the

df-Bi_2S_3/S-NCNF, indicating that the initial electrode-OH^- state can easily occur on the surface of the dr-Bi_2S_3/S-NCNF electrode to accelerate the following Faradaic reaction:

$$Bi_2S_3 + OH^- \rightarrow Bi_2S_3OH + e^- \quad (1)$$

Finally, the 3D network of dr-Bi_2S_3/S-NCNF electrode, stacked by highly conductive surface nitrogen-doped carbon nanofibers, provides efficient pathways for fast ion-diffusion and electron-transport, making it a potential for the next generation electrode materials for use in supercapacitors.

An asymmetric supercapacitor (ASC) device was assembled by using dr-Bi_2S_3/S-NCNF composite as the negative electrode and S-NCNF as the positive electrode (Figure 6a), which is denoted as a dr-Bi_2S_3/S-NCNF//S-NCNF device. Due to the collective contribution of the electric double-layer capacitance and pseudocapacitance, an asymmetric supercapacitor can achieve a higher operating voltage of 1.35 V. The CV shape (Figure 6b) can still be seen clearly even at a high scan rate of 200 mV s^{-1}, reflecting the fast charge-discharge properties of the ASC. This performance is in agreement with the galvanostatic charge-discharge curves at various current densities from 1 to 8 A g^{-1} (Figure 6c). In addition, the specific capacitances based on the total mass of ASC can be calculated based on the galvanostatic charge-discharge (GCD), the typical data of which are plotted in Figure 6d. The ASC device displays a high specific capacitance of 87.8, 81.1, 71.2, and 60.7 F g^{-1} at various current densities of 1, 2, 4, and 8 A g^{-1}, respectively. It should be noted that this device also displays good capacitance retention of 69.1%, which is closely related to the unique structure constructed by surface nitrogen-doped carbon nanofibers and bismuth sulfide nanoparticles with sulphur deficiencies on its surface.

The energy and power densities of the as-fabricated device were also calculated based on the galvanostatic discharge plots in Figure 6c (based on Eqs. (3) and (4)). Impressively, with an acceptable operating voltage of 1.35 V, the as-fabricated dr-Bi_2S_3/S-NCNF//S-NCNF asymmetric supercapacitor device exhibits a maximum energy density of 22.2 Wh kg^{-1} at a power density of 677.3 W kg^{-1}, and still maintains 16.4 Wh kg^{-1} at a high power density of 5317 W kg^{-1} (Figure 6e). This high energy storage performance is superior to those of previously reported asymmetric supercapacitor devices, such as Co_9S_8//Activated carbon(AC) device (11.2 Wh kg^{-1}, at a power density of 222.2 W kg^{-1}),[39] CuS microspheres//AC device (15.1 Wh kg^{-1}, at 392.9W kg^{-1}),[40] nickel cobalt oxide–reduced graphite oxide-activated carbon device($NiCo_2O_4$–rGO/AC) (23.3 Wh kg^{-1}, at 324.9 W kg^{-1}) [41] and Bi_2O_3//MnO_2 device (9.1 Wh kg^{-1}, at 3370 W kg^{-1}).[42] Furthermore, the durability of the as-assembled ASC device was also evaluated after 2000 cycles, and the ASC device still can keep a high capacitance retention of 118% (Figure 6f), which is comparable to those of other ASC devices. The above performance indicates that the dr-Bi_2S_3/S-NCNF//S-NCNF electrodes are promising candidates for the next-generation energy storage applications.

3. Conclusions

In summary, the defect-rich Bi_2S_3 was fabricated on surface nitrogen-doped carbon nanofibers *via* a simple solvothermal method followed by high-temperature annealing. The sulphur deficiency was successfully introduced into Bi_2S_3 by the annealing treatment. The dr-Bi_2S_3/S-NCNF composite exhibits superior electrochemical performance with an enhanced specific capacitance of 466 F g^{-1} at a discharge current

density of 1 A g^{-1}, a high capacitance retention of 64.1% even at a high discharge current density of 8 A g^{-1}, and excellent cycling stability of 81.5% retention after 1000 cycles. The high performance of dr-Bi_2S_3/S-NCNF electrode originates from its unique hierarchical structure of surface nitrogen-doped carbon nanofibers with well anchored sulphur-defect bismuth sulfides, leading to a reduced OH^- adsorption energy of -3.15 eV as assessed by density functional theory calculation. An asymmetric supercapacitor is assembled by using dr-Bi_2S_3/S-NCNF composite as negative electrode and S-NCNF as positive electrode, which exhibits a wide potential window between 0 ~ 1.35 V with a high energy density of 22.2 Wh kg^{-1} at a power density of 677.3 W kg^{-1}, demonstrating its potential applications in high-performance energy storage devices.

4. Experimental section

Materials. Polyacrylonitrile (PAN) (M_w = 150000 g mol^{-1}) was purchased from Sigma-Aldrich. *N*,*N*-dimethylformamide (DMF), bismuth nitrate pentahydrate [($Bi(NO_3)_3 \cdot 5H_2O$], and thiourea were all purchased from Sinopharm Chemical Reagent Co. All the other reagents were purchased from Sinopharm Chemical Reagent Co. Ltd and used as received without further purification.

Preparation of hybrid membranes. The preparation process of nitrogen-doped nanofiber hybrid membranes is illustrated in Figure 2a. The PAN nanofiber membrane was first prepared through a facile single-nozzle electrospinning technique using a commercial electrospinning system (UCALERY Beijing Co., Ltd, China).

Typically, 0.5 g of PAN and 0.25 g of urea were dissolved in 4.25 g of DMF at room temperature under magnetic stirring to form a viscous homogeneous precursor solution and then loaded into a 5 mL plastic syringe. The electrospinning process was carried out at a high voltage of 20 kV at a feeding rate of 0.1 mm min^{-1} through a stainless-steel needle, which had an inner diameter of 0.5 mm. The urea-containing polyacrylonitrile (u-PAN) nanofiber membranes were positioned 21 cm away from the aluminum drum collector. Then, the pre-oxidized process of the generated u-PAN nanofiber membrane was generated at 180 °C in air atmosphere for 1 h with a heating rate of 1 °C min^{-1}. The pre-oxidized u-PAN membranes were further carbonized in a conventional tube furnace under a nitrogen atmosphere at 800 °C for 2 h with a heating rate of 5 °C min^{-1}, and are denoted as NCNF. The carbonization process of surface nitrogen-doped carbon nanofiber (S-NCNF) was the same as NCNF process, except by adding an external urea precursor with a mass ratio of 5:1 (u-PAN to urea). In addition, pure CNF was obtained by a direct pre-oxidization and carbonization processes of the electrospun PAN nanofiber membrane.

Preparation of Bi_2S_3/S-NCNF hybrid composites. In a typical synthesis, 0.97 g of $Bi(NO_3)_3$ and 0.23 g of thiourea were separately dissolved in a mixed solvent of 25 mL ethylene glycol and 15 mL ethanol. Then, the as-prepared S-NCNF membranes were immersed in the above mixed solution, and then transferred into an 80 mL Teflon-lined stainless-steel autoclave for hydrothermal reaction (180 °C, 18 h). After cooling to room temperature, the sample was washed with ethanol and distilled water several times, then dried at 80 °C overnight. The obtained sample was denoted as defect-free bismuth sulfides/surface nitrogen-doped carbon nanofiber

(df-Bi_2S_3/S-NCNF) composite. After high-temperature annealing treatment of df-Bi_2S_3/S-NCNF composite at 450 °C for 10 h, the defect-rich bismuth sulfides/surface nitrogen-doped carbon nanofiber (dr-Bi_2S_3/S-NCNF) composite was successfully synthesized. Furthermore, pure Bi_2S_3 powder was prepared *via* the same steps for comparison. The overall synthesis procedure for Bi_2S_3/S-NCNF composites is shown in Figure 2a.

Materials characterization: The morphology of the nitrogen-doped carbon nanofibers and Bi_2S_3/CNF hybrid composites was observed by field-emission scanning electron microscopy (FESEM, Ultra 55) and transmission electron microscopy (TEM, Tecnai G2 20 TWIN). X-ray diffraction (XRD) patterns were measured using an X'Pert Pro X-ray diffractometer equipped with Cu Kα radiation (λ = 0.1542 nm) at a current of 40 mA and voltage of 40 kV. The Raman spectra were collected using a LabRAM-HR Confocal Laser Micro Raman Spectrometer with a 532 nm laser diode as the excitation source. X-ray photoelectron spectroscopy (XPS) analyses were made with a VG ESCALAB 220I-XL device. The curve fitting of all XPS spectra was accomplished using XPS Peak 4.1 software. All XPS spectra were corrected according to the C1s line at 284.6 eV, while curve fitting and background subtraction were accomplished using the RBD AugerScan 3.21 software provided by RBD Enterprises. Thermogravimetric analysis (TGA, Pyris 1 TGA, Perkin Elmer) was performed in air from 100 °C to 800 °C at a heating rate of 10 °C min^{-1} in order to measure the mass content of Bi_2S_3 in the composites. EIS was performed using a CHI 660D electrochemistry workstation by applying AC amplitude of 5 mV over the frequency ranged from 100 kHz to 10 mHz.

Theoretical calculation: DFT computations were performed using the plane-wave technique implemented in Vienna *ab initio* simulation package (VASP). The

projector-augmented plane wave (PAW) approach[43] was applied to describe the ion−electron interactions. The generalized gradient approximation (GGA) expressed by Perdew, Burke and Ernzerhof (PBE)[44] and a 500 eV cutoff for the plane-wave basis set were adopted in all computations. The geometry optimizations were performed by using the conjugated gradient method, and the convergence threshold was set to be 10^{-5} eV in energy and 10^{-3} eV/Å in force. The Brillouin zone was sampled with an 8×6×1 centered k-points grid.[45]

Electrochemical measurements: Electrochemical measurements were carried out in 6 M KOH aqueous solution on an electrochemical working station (CHI600D, Chenhua Instruments Co. Ltd., Shanghai) with a standard three-electrode setup where Ag/AgCl as the reference electrode and Pt wire counter electrode, respectively. Cyclic voltammograms (CVs) under various scan rates were obtained from −0.95 to -0.4 V and -0.5 to 0.4 V for N-doped nanofibers and Bi_2S_3/CNF composites, respectively. Galvanostatic charge-discharge (GCD) testing was performed under different current densities between −0.95 to -0.4 V and -0.5 to 0.4 V for Bi_2S_3/CNF composites and N-doped carbon nanofibers, respectively. The electrochemical impedance spectroscopy (EIS) measurements were conducted by using a CHI 660D electrochemistry workstation by applying an AC amplitude of 5 mV in the frequency ranging from 10 mHz to 100 kHz. Specific capacitance of the electrodes can be calculated from galvanostatic charge-discharge curves according to the following equation:

$$c = \frac{I \times \Delta t}{m \times V} \qquad (2)$$

where I is the current (A), V is the potential (V), m is the mass of electroactive materials (g), and Δt is the discharge time (s).

The asymmetric supercapacitor (ASC) was constructed from a two-electrode setup by using Bi_2S_3/S-NCNF composites as the negative electrode material and doped nanofibers as the positive electrode material. It is significant to balance the capacitance according to the specific capacitances obtained from the three-electrode system of the two electrodes. The mass-ratio of negative electrode and positive electrode was decided according to the charge balance equation (5). Galvanostatic charge–discharge curves were measured at different current densities varied from 1 to 8 A g^{-1} to evaluate the energy density and power density of the asymmetric supercapacitor by using Equations (3) and (4):

$$E = \frac{1}{2} \times C \times V^2 \quad (3)$$

$$P = \frac{E}{\Delta t} \quad (4)$$

$$\frac{m_+}{m_-} = \frac{C_- \times V_-}{C_+ \times v_+} \quad (5)$$

where C is the specific capacitance (F g^{-1}), V is the potential (V), $\triangle$t is the discharge time (s), E is the energy density (Wh kg^{-1}), and P is the power density (W kg^{-1}).

Supporting Information

Supporting Information is available from the Wiley Online Library or from the author.

Acknowledgements

The authors are grateful for the financial support from the National Natural Science Foundation of China (51373037, 51433001, and 21604010), and the Program of

Shanghai Academic Research Leader (17XD1400100) supported by Shanghai Education Development Foundation and Shanghai Municipal Education Commission and Engineering and Physical Sciences Research Council (EPSRC, EP/L015862/1).

Received: ((will be filled in by the editorial staff))
Revised: ((will be filled in by the editorial staff))
Published online: ((will be filled in by the editorial staff))

References:

[1] N. Choudhary, C. Li, J. Moore, N. Nagaiah, L. Zhai, Y. Jung, J. Thomas, *Adv. Mater.* **2017**, 29, 1605336.

[2] F. Cao, M. Zhao, Y. Yu, B. Chen, Y. Huang, J. Yang, X. Cao, Q. Lu, X. Zhang, Z. Zhang, *J. Am. Chem. Soc.* **2016,** 138, 6924.

[3] L. Wang, X. Feng, L. Ren, Q. Piao, J. Zhong, Y. Wang, H. Li, Y. Chen, B. Wang, *J. Am. Chem. Soc.* **2015**, 137, 4920.

[4] C. Liu, F. Li, L. P. Ma, H. M. Cheng, *Adv. Mater.* **2010**, 22, E28.

[5] M. F. El-Kady, R. B. Kaner, *Nat. Commun.* **2013**, 4, 1475.

[6] J. Ni, X. Bi, Y. Jiang, L. Li, J. Lu, *Nano Energy* **2017**, *3*4, 356.

[7] L. Li, N. Sun, Y. Huang, Y. Qin, N. Zhao, J. Gao, M. Li, H. Zhou, L. Qi, *Adv. Funct. Mater*. **2008**, 18, 1194.

[8] J. Tang, A. P. Alivisatos, *Nano Lett.* **2006**, 6, 2701.

[9] J. Xie, H. Zhang, S. Li, R. Wang, X. Sun, M. Zhou, J. Zhou, X. W. D. Lou, Y. Xie, *Adv. Mater*. **2013**, 25, 5807.

[10] Y. Tong, P. Chen, M. Zhang, T. Zhou, L. Zhang, W. Chu, C. Wu, Y. Xie, *ACS Catal*. **2017**, 8, 1.

[11] L. Xu, Q. Jiang, Z. Xiao, X. Li, J. Huo, S. Wang, L. Dai, *Angew. Chem. Int. Ed.* **2016**, 128, 5363.

[12] R. Liu, L. Ma, G. Niu, X. Li, E. Li, Y. Bai, G. Yuan, *Adv. Funct. Mater*. **2017**, 27,

29.

[13] T. Zhai, S. Xie, M. Yu, P. Fang, C. Liang, X. Lu, Y. Tong, *Nano Energy* **2014**, 8, 255.

[14] S. Liu, J. Xu, J. Zhu, Y. Chang, H. Wang, Z. Liu, Y. Xu, C. Zhang, T. X. Liu, *J. Mater. Chem. A* **2017**, 5, 19997.

[15] X. L. Ning, F. Li, Y. Zhou, Y. E. Miao, C. Wei, T. X. Liu, *Chem. Eng. J.* **2017**, 328, 599.

[16] K. Wang, J. Yang, J. Zhu, L. Li, Y. Liu, C. Zhang, T. X. Liu, *J. Mater. Chem. A* **2017**, 5, 11236.

[17] L. F. Chen, Z. H. Huang, H. W. Liang, W. T. Yao, Z. Y. Yu, S. H. Yu, *Energy Environ. Sci.* **2013**, 6 3331.

[18] F. L. Lai, Y. E. Miao, Y. P. Huang, T. S. Chung, T. X. Liu, *J. Phys. Chem. C* **2015**, 119, 1344.

[19] Y. Tang, B. L. Allen, D. R. Kauffman, A. Star, *J. Am. Chem. Soc.* **2009**, 131, 13200.

[20] L. F. Chen, Z. H. Huang, H. W. Liang, H. L. Gao, S. H. Yu, *Adv. Funct. Mater*. **2014**, 24, 5104.

[21] Y. Cheng, L. Huang, X. Xiao, B. Yao, L. Yuan, T. Li, Z. Hu, B. Wang, J. Wan, J. Zhou, *Nano Energy* **2015**, 15, 66.

[22] J. Yang, J. Xie, X. Zhou, Y. Zou, J. Tang, S. Wang, F. Chen, L. Wang, *J. Phys. Chem. C* **2014**, 118, 1800.

[23] S. Liu, Z. Cai, J. Zhou, A. Pan, S. Liang, *J. Alloys Compd.* **2017**, 715, 432.

[24] Z. Zhang, L. Wang, Y. Li, Y. Wang, J. Zhang, G. Guan, Z. Pan, G. Zheng, H. Peng, *Adv. Energy Mater.* **2016**, 1601814.

[25] H. W. Liang, Z. Y. Wu, L. F. Chen, C. Li, S. H. Yu, *Nano Energy* **2015**, 11, 366.

[26] F. L. Lai, Y. E. Miao, Y. P. Huang, Y. Zhang, T. X. Liu, *ACS Appl. Mater. Interfaces* **2015**, 8, 3558.

[27] L. Huang, Q. Guan, J. Cheng, C. Li, W. Ni, Z. Wang, Y. Zhang, B. Wang, *Chem. Eng. J*. **2018**, 334, 682.

[28] S. Wang, X. Li, Y. Chen, X. Cai, H. Yao, W. Gao, Y. Zheng, X. An, J. Shi, H. Chen, *Adv. Funct. Mater*. **2015**, 27, 2775.

[29] D. M. Sim, M. Kim, S. Yim, M. J. Choi, J. Choi, S. Yoo, Y. S. Jung, *ACS Nano, **2015***, 9, 12115.

[30] Y. Xu, L. Wang, X. Liu, S. Zhang, C. Liu, D. Yan, Y. Zeng, Y. Pei, Y. Liu, S. Luo, *J. Mater. Chem. A* **2016**, 4, 16524.

[31] H. Li, C. Tsai, A. L. Koh, L. Cai, A. W. Contryman, A. H. Fragapane, J. Zhao, H. S. Han, H. C. Manoharan, F. Abild-Pedersen, J. K. Norskov, X. Zheng, *Nat. Mater.* **2016**, 15, 48.

[32] Q. Meng, K. Qin, L. Ma, C. He, E. Liu, F. He, C. Shi, Q. Li, J. Li, N. Zhao, *ACS Appl. Mater. Interfaces* **2017**, 9, 30832.

[33] R. R. Salunkhe, Y. Kamachi, N. L. Torad, S. M. Hwang, Z. Sun, S. X. Dou, J. H. Kim, Y. Yamauchi, *J. Mater. Chem. A* **2014**, 2, 19848.

[34] Z. Y. Sui, Y. N. Meng, P. W. Xiao, Z. Q. Zhao, Z. X. Wei, B. H. Han, *ACS Appl. Mater. Interfaces* **2015**, 7, 1431.

[35] G. Qu, S. Jia, H. Wang, F. Cao, L. Li, C. Qing, D. Sun, B. Wang, Y. Tang, J. Wang, *ACS Appl. Mater. Interfaces* **2016**, 8, 20822.

[36] G. Nie, X. Lu, J. Lei, L. Yang, C. Wang, *Electrochim. Acta* **2015**, 154, 24.

[37] B. Pandit, G. K. Sharma, B. R. Sankapal, *J. Colloid Interface Sci.* **2017**, 505, 1011.

[38] S. Vadivel, A. N. Naveen, V. Kamalakannan, P. Cao, N. Balasubramanian, *Appl. Surf. Sci.* **2015**, 351, 635.

[39] F. Zhu, M. Yan, Y. Liu, H. Shen, Y. Lei, W. Shi, *J. Mater. Chem. A* **2017**, 5 22782.

[40] W. Fu, W. Han, H. Zha, J. Mei, Y. Li, Z. Zhang, E. Xie, *Phys. Chem. Chem. Phys*. **2016**, 18, 24471.

[41] X. Wang, W. S. Liu, X. Lu, P. S. Lee, *J. Mater. Chem.* **2012**, 22, 23114.

[42] H. Xu, X. Hu, H. Yang, Y. Sun, C. Hu, Y. Huang, *Adv. Energy Mater*. **2014**, 1401882.

[43] P. E. Blochl, *Phys. Rev. B* **1994**, *50*, 17953.

[44] J. P. Perdew, K. Burke, M. Ernzerhof, *Phys. Rev. Lett.* **1996**, *77*, 3865.

[45] H. J. Monkhorst, J. D. Pack, *Phys. Rev.* **1976**, *13*, 5188.

Figure captions:

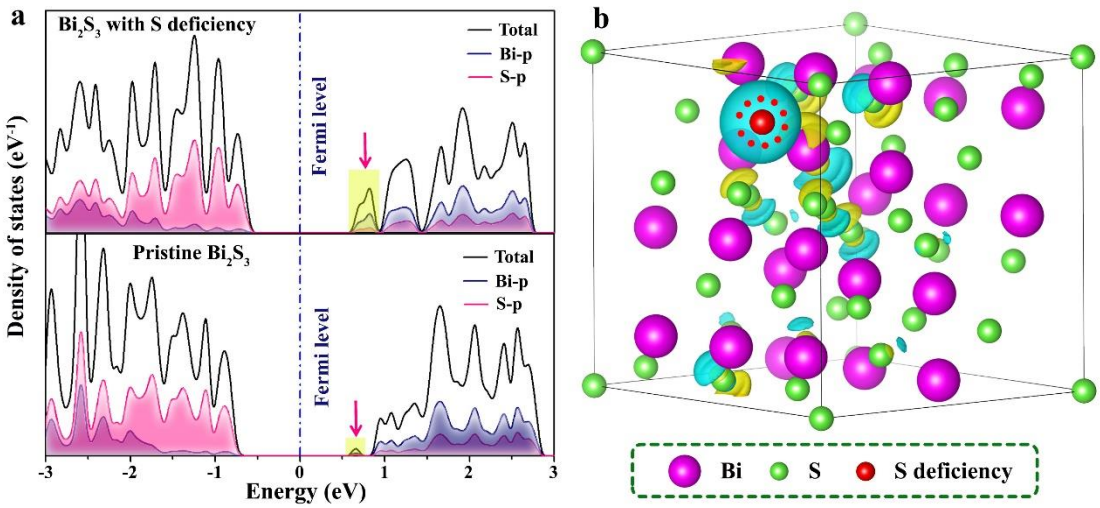

Figure 1. a) Calculated DOS for sulphur-deficient Bi_2S_3, and pristine Bi_2S_3. The shadowed region highlights the increased DOS at the conduction band edge of sulphur-deficient Bi_2S_3. b) The differential charge density of sulphur-deficient Bi_2S_3.

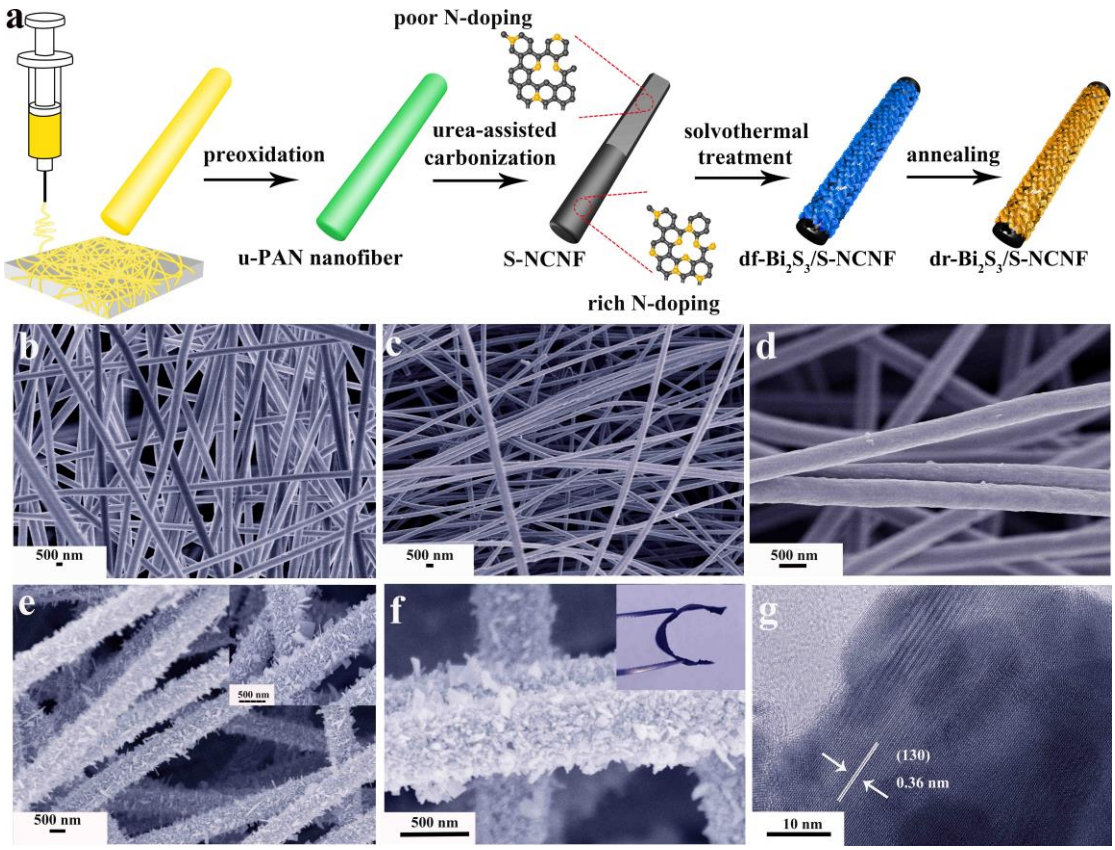

Figure 2. a) Schematic illustration of the preparation of dr-Bi_2S_3/S-NCNF composite. The FESEM images of b) the electrospun u-PAN nanofibers, c, d) S-NCNF with different magnification, and e, f) dr-Bi_2S_3/S-NCNF composite with different magnification (Inset in Figure 2e: the FESEM image of df-Bi_2S_3/S-NCNF composite; Inset in Figure f: the digital photo of flexible dr-Bi_2S_3/S-NCNF composite membrane). g) HRTEM image of dr-Bi_2S_3/S-NCNF composite.

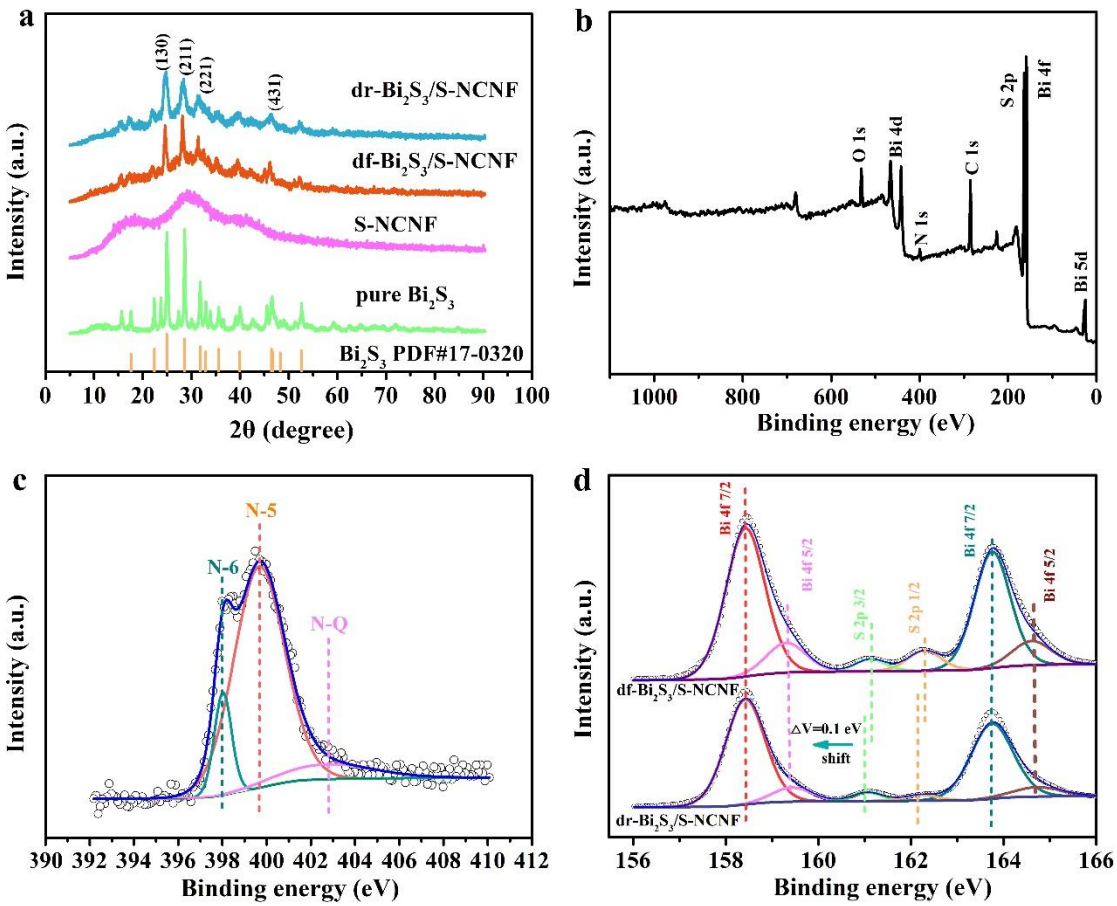

Figure 3. a) X-ray diffraction patterns of dr-Bi_2S_3/S-NCNF, df-Bi_2S_3/S-NCNF composites, S-NCNF and pure Bi_2S_3. b) XPS survey spectrum of dr-Bi_2S_3/S-NCNF composite. c) High resolution spectrum of the N 1s peak of dr-Bi_2S_3/S-NCNF composite. d) High resolution spectra of the Bi 4f and S 2p peaks of dr-Bi_2S_3/S-NCNF, df-Bi_2S_3/S-NCNF composites.

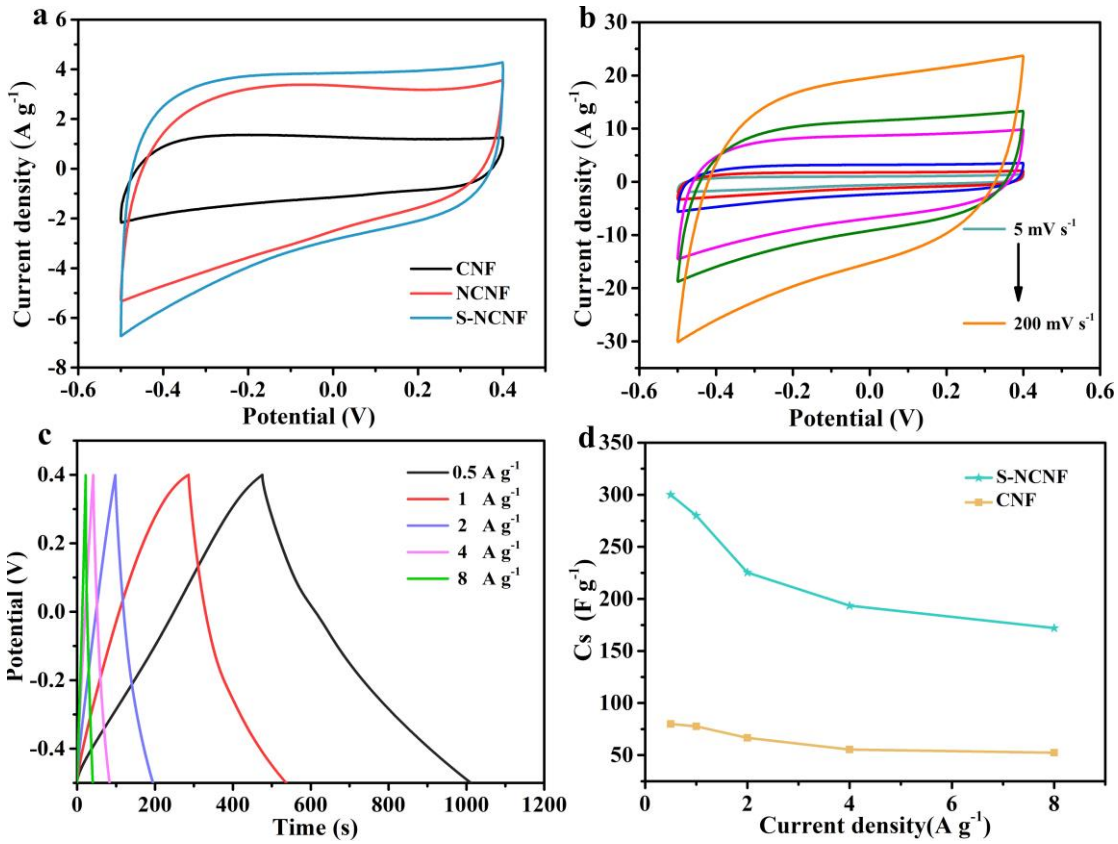

Figure 4. a) CV curves of CNF, NCNF and S-NCNF at a scan rate of 20 mV s^{-1}. b) CV curves of S-NCNF at various scan rates. c) Galvanostatic charge-discharge curves at various current densities for S-NCF nanofibers. d) Specific capacitance of S-NCNF and CNF nanofibers at various current densities.

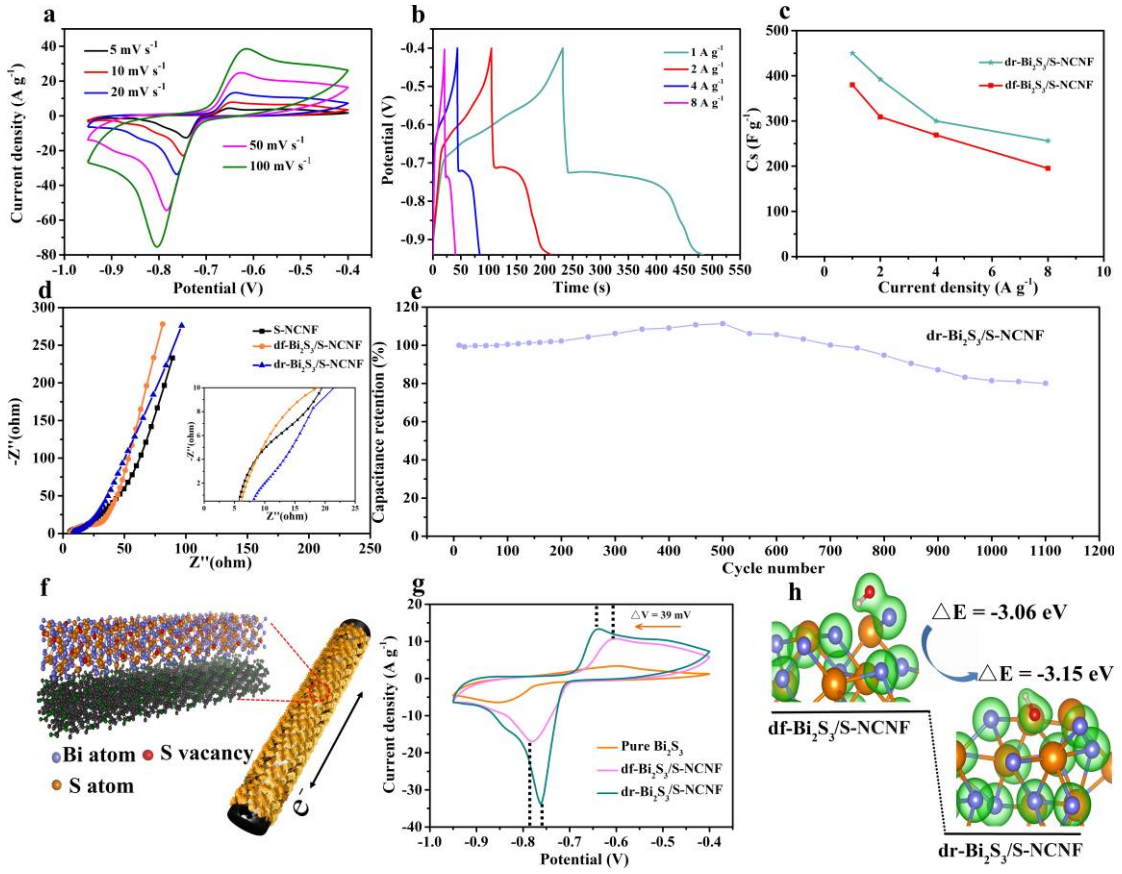

Figure 5. a) CV curves of dr-Bi_2S_3/S-NCNF composite at various scan rates. b) Galvanostatic charge-discharge curves at various current densities for dr-Bi_2S_3/S-NCNF composite. c) Specific capacitance of dr-Bi_2S_3/S-NCNF composite at various current densities. d) Nyquist plots of S-NCNF, df-Bi_2S_3/S-NCNF, dr-Bi_2S_3/S-NCNF. e) The long-term cycling performance of dr-Bi_2S_3/S-NCNF composite at a scan rate of 200 mV s^{-1}. f) Illustration of the electrochemical processes for dr-Bi_2S_3/S-NCNF composite. g) CV curves of pure Bi_2S_3, df-Bi_2S_3/S-NCNF, dr-Bi_2S_3/S-NCNF composites at a scan rate of 20 mV s^{-1}. h) Schematic reaction pathway of dr-Bi_2S_3/S-NCNF.

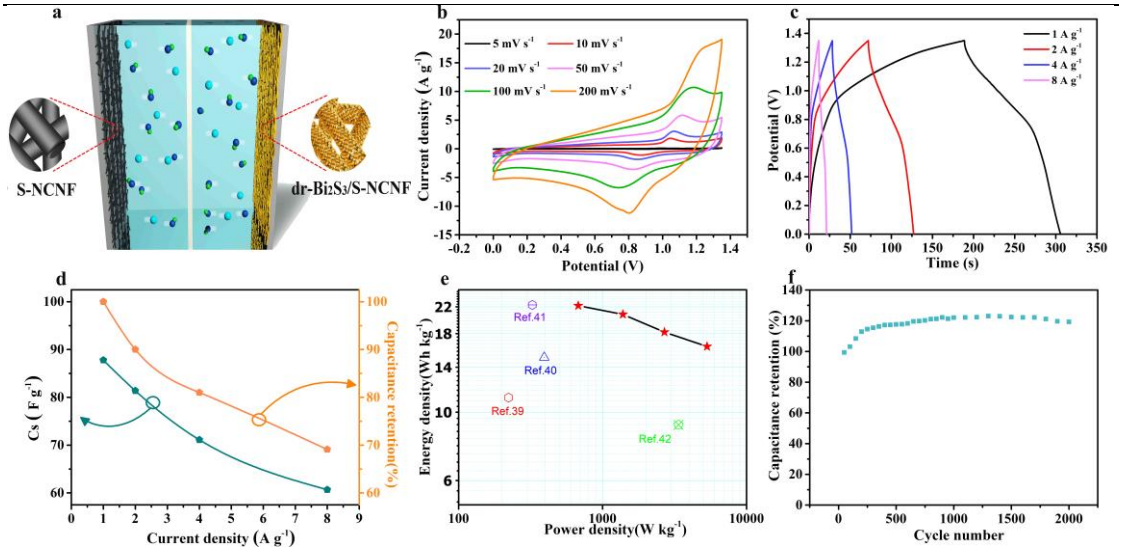

Figure 6. a) Schematic of the assembled structure of an asymmetric supercapacitor based on dr-Bi_2S_3/S-NCNF composite as negative electrode material and S-NCNF as positive electrode material. b) CV curves at various scan rates, and c) galvanostatic charge-discharge curves at various current densities for the assembled asymmetric supercapacitor. d) Specific capacitance and the corresponding capacitance retention of the as-assemble dr-Bi_2S_3/S-NCNF//S-NCNF ASC device at different current densities. e) Ragone plots of the as-assembled ASC device and recently reported values for comparison. f) The long-term cycling performance of the device at a scan rate of 200 m V s^{-1}.